Advances in Science and Technology Research Journal

Advances in Science and Technology Research Journal, 2025, 19(3), 362–380
https://doi.org/10.12913/22998624/199509
ISSN 2299-8624, License CC-BY 4.0

Received: 2024.12.06
Accepted: 2025.01.14
Published: 2025.02.01

Skin sensors modelling for smarter and safer autonomous systems

Artur Wiliński[1*], Imed El Fray[2]

[1] Faculty of Applied Informatics and Mathematics, Warsaw University of Life Sciences, Nowoursynowska 159, Warsaw, Poland
[2] Faculty of Computer Sciences and Information Technology, West Pomeranian University of Technology, Al. Piastów 17, Szczecin, Poland
* Corresponding author's e-mail: artur_wilinski@sggw.edu.pl

ABSTRACT

The increasing integration of intelligent sensors into autonomous systems, especially in the context of IoT, requires comprehensive and safer solutions, additionally adaptable and reliable. Modelling their dynamic behavior in complex environments remains a challenge. This study fits into these areas and computationally models capacitive and inductive skin sensors to ensure robust functionality and seamless IoT integration. This study introduces a robust model of IoT-integrated multi-sensors, demonstrating their ability to convert capacitance changes in the environment into current signals and shape them for control purposes, which is crucial for smart skin sensor systems. Interval calculations were used to optimize the parameters of the integrated sensors. This analysis highlighted their sensitivity to touch and environmental conditions, which is critical for developing safer and more intelligent responses of such systems. It is shown how changes in the sensor-object distance affect the optimization of the integrated sensor behavior, which is essential for managing uncertainty in real-world applications, ensuring reliable and consistent performance. The authors proposed a model for integrating an intelligent skin sensor with an autonomous IoT system. This model shows significant potential for miniaturization, integration with nanogenerators, and scalability, making it particularly suitable for IoT applications. The study confirmed the practical usefulness of these models in designing intelligent and autonomous sensor arrays capable of robust and trouble-free operation in complex, dynamic, and safety-critical IoT-enabled environments.

Keywords: autonomous systems, human-machine interface, intelligent skin sensors, wearable sensors, e-skin, IoT, flexible sensor, security.

INTRODUCTION

Intelligent skin sensors (ISS) imitate the capabilities of human skin, such as touch response, sensing multiple elements of the environment at once, such as liquid, heat, and structure, distinguishing pressure, temperature, humidity, or remote proximity of objects. Their flexibility and sensitivity make them suitable for applications in automation, robotics, and computer science that interact with the Internet of Things (IoT). The aim of this study is to develop general models of smart skin sensors on array structures, focusing on their applications in intelligent autonomous systems integrated with the IoT. Navigation in dynamic environments using such sensors allows for real-time detection of changes in the environment. In the paper [1] provides an overview of materials and structures used in electronic skin and their functions in the context of robotics and IoT applications. The design, manufacturing, and application processes of multi-responsive flexible sensors and the challenges of manufacturing these sensors for the next generation of e-skin and wearable electronics presents in the work [2]. The main approaches used to construct more flexible and stretchable sensors and the efforts to provide high-performance e-skin as well as the urgent needs for various types of artificial intelligent e-skins for personalized medicine highlights in the

paper [3]. The system of powering such systems is always relevant and in the work [4] recent progress on flexible nanogenerators for mechanical energy harvesting toward self-powered systems, including flexible piezoelectric and triboelectric nano-generator, is reviewed. In the field of AI review presented in [5] explores the confluence of e-skins and machine learning to build autonomous soft robots, integrated with capabilities for informative. The review presented in [6] summarizes technologies using soft sensors and actuators, as well as power sources based on flexible and stretchable electronics for artificial electronic skin, wearable biosensors and stimulators. Inspired by natural biological systems soft robots have been developed, showing tremendous potential in real-world applications because of their intrinsic softness and deformability using intelligent e-skin sensors [7]. The specific hybrid of electronic skins and machine learning is extensively studied to create effective biomimetic robotic systems. This study presents a shape-sensing electronic skin that can recognize surface conformations with minimal interference from pressing, stretching, or other surrounding stimuli. It is integrated with soft robots to reconstruct their shape during movement, serving as a kinesthetics sense with deep sensation. The next review [8] examines the latest developments in feedback sensing technologies for soft robots. In the paper [9] five typical skin-like electronics with sensitivities analogous to the human senses (olfactory, visual, auditory, tactile, and gustatory senses) and their potential applications in IoT. The work [10] presents progress in electronic skin or e-skin research is reviewed, focusing on technologies needed in skin-attachable electronics, robotics, prosthetics and some perspectives on challenges and opportunities for research in flexible hybrid electronics. The materials with intrinsic stretchability and self-healing properties are of great importance for several reasons. First, since e-skin will be exposed to prolonged stresses of various kinds and needs to be conformally adhered to irregularly shaped surfaces. Second, in different applications tactile sensing capability by the detection of pressure, strain, slip, force vector, and temperature are important for health monitoring in skin attachable devices. Next review in [11] mainly focuses on the representative advances of the flexible sensors for health monitoring, such as applies skin-like pressure and strain sensors integrated with the human body owing to their excellent flexibility and adaptability. The representations of flexible sensors with the favourable biocompatibility and self-driven properties are also introduced, important from the point of view of implantable bioelectronics. The other proposed approach [12], combined with a deep neural network, enables us to freely select the sensing mode according to our purpose, where artificial skins or flexible pressure sensors can transduce tactile stimuli to quantitative electrical signals by mimicking the perceptual functions of human cutaneous mechano-receptors. The paper [13] describes the reverse design of artificial skins using machine learning on small data sets, which allows for efficient creation of solutions adapted to different materials. The articles [14, 15] present highly sensitive optical skin in which the primary sensory elements are optically driven, using the simple construction of the sensors by embedding glass micro/nanofibers in thin layers of polydimethylsiloxane. This optical sensors show ultrahigh sensitivity, low detection limit and fast response 10μs for pressure sensing, significantly exceeding the performance metrics of state-of-the-art electronic skins. Electromagnetic interference free detection of high-frequency vibrations, wrist pulse and human voice are realized. Many publications provide up-to-date information on the latest developments in the field of smart skin sensors in the context of their applications in robotics and IoT. Skin offers a diagnostic interface rich with vital biological signals from the inner organs, blood vessels, muscles, and dermis/epidermis. Soft, flexible, and stretchable electronic devices provide a novel model to interface with soft tissues for robotic feedback and control, regenerative medicine, and continuous health monitoring [16]. The authors use the term “lab-on-skin” to describe a set of electronic devices that have physical properties resembling skin, such as thickness, thermal mass, elastic modulus, and water vapor permeability. These microsystems can conformally laminate onto the epidermis to mitigate motion artifacts and mechanical property mismatches of rigid electronics, providing accurate, non-invasive, long-term, and continuous health monitoring. Therefore, it is also perfect for smartphone skins. Self-powered tactile sensors do not require an external power source to drive, which makes the entire system more flexible and lightweight [17]. Therefore, they are excellent for mimicking the tactile perception functions for wearable health monitoring and ideal electronic

skin (e-skin) for intelligent robots. The review [18] discusses the materials, structural designs, and integrated techniques for e-skins and how to optimize the performance is also discussed. The existing flexible sensing materials and microstructures, including flexible stimuli-responsive materials and response- and stretchability-enhanced microstructures, are reviewed in the paper [19]. A typical skin-like electronics with sensitivities analogous to the human senses (olfactory, visual, auditory, tactile, and gustatory senses) and their corresponding applications (gas, light, chemical composition, sound, and mechanical signal monitoring) are introduced. The perspectives of challenges and opportunities for future research on flexible hybrid electronics are indicated. Learning from nature provides endless inspiration for scientists to invent new materials and devices and the work [20] have the review state-of-the-art technologies in flexible electronics, with a focus on bio-inspired smart skins. This review focuses on the development of e-skin for sensing a mechanical loads, temperature, light, and biochemical cues, with a trend of increased integration of multiple functions. It highlights the most recent advances in flexible electronics inspired by animals such as chameleons, squids, and octopi whose bodies have remarkable camouflage, mimicry, or self-healing attributes. In the next article [21] it was emphasized that human skin is a large-area, multi-point, multi-modal stretchable sensor that has inspired the development of electronic skin for humanoids, enabling them to simultaneously detect pressure and thermal distributions. In this paper, authors report the recent progress of stretchable thin-film sensors that are developed for application to robotics and wearables. In the study [22], design guidelines for robotic gloves are proposed, because e-skin is playing an increasingly important role in medicine, health detection, robotic teleoperation, and human-machine interaction, but most e-skins currently lack the integration system of signal acquisition and transmission modules. Based on this developed e-skin system and developed robotic multi-fingered hand, authors conduct gesture recognition and robotic multi-fingered teleoperation experiments using deep learning techniques [23]. A unified e-skin system can enable IoT communication across the entire body, positioning humans as integral nodes in the Internet of Everything, streamlining information transmission for greater efficiency [24]. However, how to ensure stability and long-term reliability while maintaining a highly sensitive, flexible, and stretchable is a challenge. Another work has shown that achieving high sensing performance comparable to our skin is still a huge challenge [25]. Basic strategies are here presented to enable e-skins to perform functions such as strain sensing, pressure sensing, shear sensing, temperature sensing, humidity sensing, and self-healing.

Above, only a cross-section and a small fragment of the publications concerning the area base for intelligent skin sensors is cited. Next, the specification of the sensors that are the basis of this work is presented.

MATERIALS AND METHODS

Advancements and comparison

The flexibility, sensitivity, and integration capabilities make ISS's suitable for applications in robotics, wearables, and industrial systems. Smart Skins in technology enhance telemedicine by transmitting medical data and improve robotics with precise manipulation, safety, and real-time adjustments. Humanoid and mobile robots use these sensors for touch interaction, obstacle detection, rescue operations, and advanced medical devices. In IoT and robotics, smart sensors boost real-time operation, safety, and accuracy, enabling remote monitoring and control. Smartphones leverage smart sensors for touch detection, pressure measurement, and proximity features. Acting as IoT hubs, they enhance user interaction, safety, and personalized medicine through advanced automation. The authors compared of the ISS and traditional sensors across several aspects: design and materials (Table 1), functionality (Table 2), applications (Table 3), communication (Table 4), energy efficiency (Table 5), durability (Table 6), and cost (Table 7). ISS's provide advanced functionalities beyond traditional sensors, offering improved design, materials, and integration.

Intelligent skin sensors offer advanced functionalities that are significantly different from traditional sensors used in automation, IoT and robotics. Here are the key differences between them. Based on Tables 1–7 above intelligent skin sensors outperform traditional sensors in terms of multifunctionality, flexibility, energy efficiency, and the ability to integrate with IoT.

Table 1. Construction and materials

Features	Intelligent skin sensors	Traditional sensors
Flexibility	Made of flexible and stretchable materials such as polymers (e.g. PDMS, PVDF).	Usually rigid, made of metals or rigid plastics.
Complexity of construction	Multi-layer structures enabling integration of multiple functions (e.g. pressure, temperature, humidity).	Usually single-function (e.g. only pressure or temperature sensor).

Table 2. Functionality and measurement capabilities

Features	Intelligent skin sensors	Traditional sensors
Multifunctionality	They can simultaneously measure pressure, temperature, humidity, vibration, and even proximity.	Typically single-function, requiring many separate sensors for similar applications.
Sensitivity range	Very high sensitivity, enabling detection of micro-changes in the environment.	Sensitivity dependent on design, often limited to macroscale.
Stimuli response	More precise representation of mechanical and environmental stimuli, inspired by human skin.	They respond to stimuli, but without the ability to reflect complex interactions.

Table 3. Applications

Features	Intelligent skin sensors	Traditional sensors
Robotics applications	Ideal for applications in humanoid robots, grippers, and mobile devices.	Limited to rigid structures and more basic applications.
Wearable	Can be integrated with clothing and medical devices.	Rarely used in clothing or flexible applications.
Environmental monitoring	They can be used in smart buildings, monitoring many parameters simultaneously.	They require the use of many different types of sensors.

Table 4. Communication and integration

Features	Intelligent skin sensors	Traditional sensors
IoT Integration	They integrate easily with IoT systems thanks to built-in communication modules.	They require additional elements to communicate with IoT (e.g. gateways).
Modularity	They can be modular, combining multiple functions into one item.	Usually used as single components.

Table 5. Energy saving

Features	Intelligent skin sensors	Traditional sensors
Power	They can be powered by piezo-electrics or other energy-harvesting technologies.	They usually require an external power source, such as batteries or a wired power supply.
Power consumption	Very low power consumption due to advanced power management.	They consume more energy due to their less optimized design.

Table 6. Strength and durability

Features	Intelligent skin sensors	Traditional sensors
Damage resistance	Thanks to flexible materials, they are more resistant to cracking and mechanical damage.	Rigid structures may be susceptible to damage from mechanical forces.
Adaptation to the environment	Can be used in variable environmental conditions (e.g. high humidity, vibrations).	Limited ability to work in extreme conditions.

Table 7. Cost and availability

Features	Intelligent skin sensors	Traditional sensors
Cost	Higher unit cost due to advanced technology and materials.	Usually cheaper due to simpler design.
Availability	Still developing technology, available mainly in specialist applications.	Widely available in a wide range of industrial and consumer applications.

They are particularly useful in applications that require precision, flexibility, and operation in diverse environmental conditions. Traditional sensors, on the other hand, are more cost-effective, easier to implement in basic applications, and nowadays more widely available.

Demonstrative model basic concept

IoT integrates devices with the cloud for real-time monitoring, analysis, and control in automation, enabling machine condition monitoring, failure prediction, and remote management. The authors proposed a model for integrating artificial skin through the ISS (also called smart skin sensors ^{3}S) sensor with an autonomous IoT system (Fig. 1).

The integration operates as follows: ISS detects data such as touch, pressure and temperature. This data is processed by a microcontroller, which transmits the signal to an IoT gateway. The gateway then forwards the data to the cloud, where it is analyzed and visualized. Energy storage for the system is managed by supercapacitors, providing a flexible and efficient power source. Where necessary, zero-energy operation requires combining piezoelectricity with triboelectricity to increase efficiency [26-28]. Triboelectricity is a phenomenon of static electricity that occurs when two different materials come into contact with each other and are then separated, leading to the transfer of electric charges between them. Integrating smart skin sensors with IoT is key to a new generation of systems that are more autonomous, safe, and efficient. The use of these technologies in combination with predictive and data analysis systems is transforming traditional approaches to automation, laying the foundation for the smart factories of the future.

^{3}S and IoT integration

Integrating smart skin sensors ^{3}S with IoT (Fig. 1) is crucial for developing autonomous, safe, and efficient systems. Smart skin sensors advance IoT and robotics by enabling real-time operation, safety improvements, and task accuracy. In IoT, these sensors enable anomaly detection, failure prediction, and environmental monitoring, such as proximity sensors for movement detection or smart furniture for posture monitoring [29]. In healthcare, wearable sensors monitor temperature, pulse, and pressure, while telemedicine employs smart skins to transmit medical data to cloud systems. In robotics, smart skins enhance precise object manipulation, real-time grip adjustments, and safe human-robot interaction by detecting human contact and preventing injuries. They enable humanoid robots to mimic human touch for interaction and emotional communication. Mobile and medical robots benefit from these sensors for obstacle detection, collision avoidance, and improved prosthetics functionality. Surgical and rescue robots use them for precise force control and victim detection in rubble. In smartphones, they enhance touch detection, gesture recognition, and user safety. Capacitive sensors enable precise gestures, while proximity sensors manage automatic functions like screen shutdown during calls. Biometric sensors and humidity detection further improve safety and interaction, positioning smartphones as central IoT nodes in homes, businesses, and hospitals.

IoT-enabled ^{3}S security

In the context of the ^{3}S-IoT-AS, data security is a critical concern, particularly regarding the risk of data leakage. Sensitive data, such as information from fingerprint and touch force sensors, can be intercepted if not properly protected. A recommended solution is encrypting biometric data and storing it locally in secure hardware areas, such as Secure Enclave in processors. IoT devices and smartphones acting as IoT hubs, are potential targets for cyberattacks, especially when sensors communicate with other devices without sufficient security measures. To mitigate this risk, communication between IoT devices should be encrypted using protocols like TLS/SSL, and robust authorization and authentication mechanisms should be implemented [30]. Smartphones, as IoT gateways, can securely collect data from

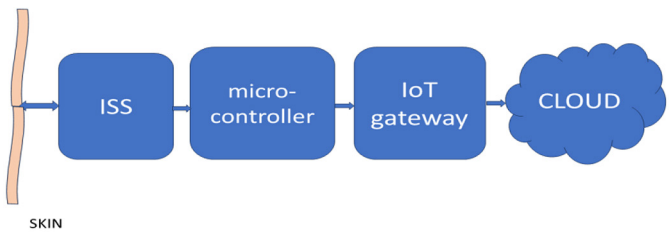

Figure 1. The integration of smart skin sensors with IoT for autonomous systems (^{3}S-IoT-AS)

automation systems and transmit it to the cloud, leveraging smart sensors [31]. These devices also cooperate with robots equipped with smart skins, which provide data on operational status. In scenarios involving touch and gesture recognition, ^{3}S can further enhance security by functioning as access authorization tools. Properly securing these systems ensures safe and efficient operation in IoT-enabled environments.

Datasets

Datasets for smart skin sensors in IoT-enabled autonomous systems should encompass a broad range of data types to support the system's development, training, and evaluation. This study uses data from sensor modelling. Sensor data capture interactions such as touch, pressure, temperature, humidity, and proximity. Data on changes in capacitance and inductance, resulting from physical interactions, supports the modelling of dynamic behavior and touch-sensitive controls or gesture. This data enhances the system's ability to interact intelligently with users and performance measures the operational efficiency and reliability of the smart skin sensor system. To ensure data integrity and user privacy, robust security measures such as encryption and anonymization must be implemented to protect sensitive biometric and operational data. These datasets collectively facilitate the design of smarter, safer, and more efficient autonomous systems.

EFHI^{3}S architecture

^{3}S are advanced sensor systems embedded in flexible, thin and often stretchable materials that mimic the properties of human skin. For some order, some explanations are needed. ^{3}S can detect various parameters as pressure, temperature, humidity and even bioelectrical signals of the body.

The capacitive or piezoelectric sensors are used to detect pressure and proximity, detecting touch and pressure in real time. Bioelectric monitoring is done using electrodes embedded in the skin that record signals. The skins can adapt to curved surfaces such as the human body or robot parts or smartphone surfaces, which makes them flexible and stretchable. the energy flow in hybrid intelligent skin sensors system (EFHI^{3}S) integrated with IoT is shown in Figure 2. Supercapacitors (Hybrid-SupLiC) are devices that store electrical energy, which combine the properties of traditional capacitors with those of batteries. Their main advantage is the ability to quickly store and release energy and an exceptionally high number of charge and discharge cycles compared to chemical batteries. Supercapacitors do not use chemical reactions to the same extent as batteries, but store energy on the principle of electrostatic charge accumulation (double layer) or through pseudo capacitance resulting from surface reactions.

In the future, this technology may play a key role in power supply system's requiring high dynamics and durability, especially in combination with other energy storage technologies. Hybrid-SupLiC provide energy to magnetic field energy storage (MagFES) via a MosFET key. The energy is stored here and decreases over time. The inductive sensor contains a coil through which an current flows. The current flow generates an alternating electromagnetic field around the coil. If the conductor is near the electromagnetic field, eddy currents are induced in the material. These currents generate their own magnetic field, which counteracts the field generated by the sensor coil. The resulting eddy currents cause a decrease in the current amplitude in the coil (due to the generation

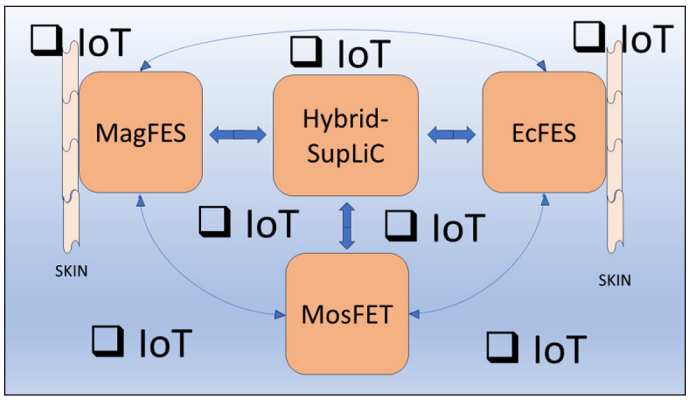

Figure 2. The energy flow in hybrid intelligent skin sensors system integrated with IoT

of energy losses) and a change in the coil impedance, in particular inductance. The sensor analyse changes in the circuit of the coil (e.g. a decrease in the amplitude or a phase shift of the current). On this basis, it is detected whether the object is in the sensor's detection field. After detecting a change in the magnetic field, the sensor generates an output signal (e.g. digital or analog). This signal can be used to control other devices, record the presence of an object, etc. The energy stored in a magnetic sensor is due to its ability to store energy in a magnetic field. In the case of an inductor coil (the main element of a magnetic sensor), this energy is described by the equation $E = 0.5LI^2$, where E is energy stored in the magnetic field [J], L is the coil inductance [H] and I is the current flowing through the coil [A]. The energy flow in the sensor can be modelled as a relationship between energy E_{IN} supplied by the voltage source, energy E_{STORE} stored in the coil and energy E_{LOSS} lost to the coil reactance and other elements. The dynamic relationship is described by the equation $E_{IN} = E_{STORE} + E_{LOSS}$. In real-world situations, we use interval calculations to account for uncertainties in key parameters: L inductance in the range $[L_{min}, L_{max}]$, X_L reactance in the range $[X_{Lmin}, X_{Lmax}]$ and input voltage V in the range $[V_{min}, V_{max}]$. The dynamic energy changes can be expressed in ranges: $E_{STORE}(t) = 0.5LI(t)^2$. The current $I(t)$ is a function of the voltage and impedance:

$$I(t) = \frac{V(t)}{R+j\omega L} \tag{1}$$

The following values were assumed for the simulation: min inductance L_{0_min} = 9e-3 [H], max inductance L_{0_max} = 11e-3 [H], Z_{L_min} = 4 [Ω], Z_{L_max} = 6 [Ω], min voltage $V_{\_min}$ = 0.9 [V], max voltage $V_{\_max}$ = 1.1 [V], current frequency f = 1e3 [Hz]. Similarly, from Hybrid-SupLiC energy is transferred to the electric field energy storage (EcFES) capacitive sensor system. The capacitive sensor works on the principle of measuring changes in electrical capacitance, which is dependent on the geometry and electrical properties of objects located near the sensor. The capacitance change is converted into an electrical signal that can be analyzed. The basic equation for such a sensor is that of a capacitor and is given by the formula

$$C = \varepsilon \frac{A}{d} \tag{2}$$

where: C is capacitance [F], ε electrical permittivity of the material ($\varepsilon = \varepsilon_0\varepsilon_r$), A is capacitor plate area [m²] and d distance between plates [m].

If a conductive or dielectric object comes close to the sensor, the permittivity (ε), distance (d) or effective area (A) changes. The electronic processing circuit reads the capacitance changes and converts them into a digital or analog signal. The capacitive sensor measures changes in capacitance C, which are related to: approaching an object (reducing the distance), changes in the dielectric (change in permittivity ε_r). In a special system, capacitance changes are converted into frequency changes:

$$f = \frac{1}{2\pi\sqrt{LC}} \tag{3}$$

or

$$f = \frac{1}{RC} \tag{4}$$

where: R and L are constant circuit elements.

Frequency is converted to voltage using rectifier or digital circuits. The V/I converter circuit is used, e.g. an operational transconductance amplifier (OTA), where $I_{OUT} = G_m V_{IN}$, where G_m is the transconductance coefficient. Once the signal has been converted into current, it can be further processed for analysis, transmission, or control. The minimum capacitance (C_{min}) results from the minimum values of ε_r, A and the maximum distance d. The maximum capacity (C_{max}) corresponds to the maximum values of ε_r, A and the minimum distance d. The capacitance range shows how parameter changes affect the possible capacitance values of the sensor. The simulation parameters were defined as: ε_0 = 8.854e-12 [F/m], ε_{r_min}=1.0, ε_{r_max}=5.0; min area A_{min}=1e-4 [m²], A_{max}=2e-4 [m²], min distance d_{min}=1e-3 [m] and max distance d_{max} = 5e-3 [m].

Sensor signal measurement

The block diagram is shown on the Figure 3. The measurement system consists of a capacitive sensor (CS) that measures capacitance changes. The oscillator (Osc.) converts capacitance changes to frequency. The frequency detector (FD) converts frequency to voltage. The $V \rightarrow I$ converter converts voltage to current. The ADC digitizes the signal for further analysis. The control unit (CU) analyses the signal and makes decisions (e.g. sending data to the IoT cloud).

Sensor peaks

In this study, the authors showed how a forced harmonic change of the sensor capacitance affects

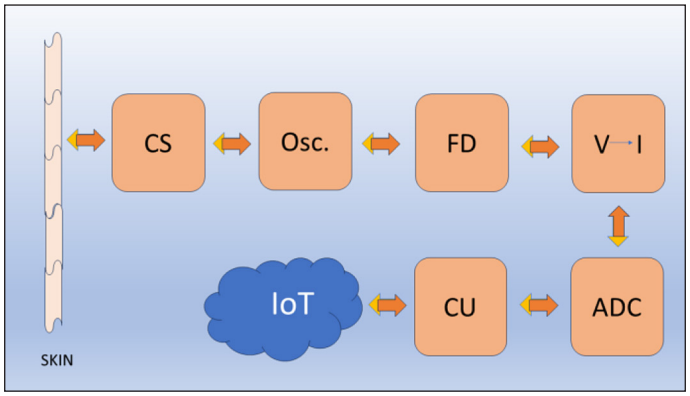

Figure 3. Converting a capacitive sensor signal to a current signal within a single element of a matrix consisting of several sensors

the corresponding current. The sensor parameters are: minimum capacitance 10e-12 [F], maximum capacitance 100e-12 [F], sampling rate 1e3 [Hz]. The nature of these sensor capacitance C_t changes clearly shows the dependence:

$$C_t = C_{min} + (C_{max} - C_{min})(0.5 + 0.5sin(2\pi 2t)). \quad (5)$$

The sensor parameters are: minimum capacitance 10e-12 [F], maximum capacitance 100e-12 [F], sampling rate 1e3 [Hz]. RC oscillator oscillations are frequency f_t versus capacitance with resistance R = 1e3 [Ω]

$$f_t = \frac{1}{2\pi RC_t} \text{ [Hz]} \quad (6)$$

Frequency to voltage conversion (f_t/V_t) with voltage normalization [0, 1]: $V_t = f_t/maxf_t$ [Hz]. The conversion of voltage into current was implemented as $I_t = G_m \cdot V_t$ [A], with transconductance coefficient G_m = 1e-3 [A/V].

Harmonic sensor capacitance

Here we will present a sensor model, based on Figure 2 and [32, 33], with a AC voltage $V(t) = V_0 \sin(2\pi ft)$, which ensures proper operation of the measurement system. For clarity, we will assume zero initial conditions for the capacitive sensor (EcFES) system $u_C(0\text{-}) = 0$ and $i_L(0\text{-}) = 0$ for inductive sensor (MagFES). The simulation parameters are: voltage amplitude V_0=5 [V], voltage frequency f = 50 [Hz], minimum capacity C_{min}=10e-12 [F], maximum capacity C_{max}=100e-12 [F], frequency of capacitance changes f_C = 2 [Hz]. The simulation assumed that the capacity changes according to the relationship:

$$C_t = C_{min} + (C_{max} - C_{min})\, sin(2\pi f_C t). \quad (7)$$

where: C_{min}, C_{max} minimum and maximum capacity, f_C frequency of capacitance changes.

The current flowing through the sensor in the capacitive branch:

$$I(t) = C(t)\frac{dV(t)}{dt} \quad (8)$$

Distance between capacitor plates

In this study we analysed how the distance between the capacitor plates affects the sensor capacitance. We assumed here that: ε_0 = 8.854e-12 [F/m], plate area A = 1e-4 [m²], min distance d_{min} = 1e-3 [m], max distance d_{max} = 5e-3 [m]. The change in distance over time is as follows:

$$d_t = d_{min} + (d_{max} - d_{min})\,(0.5 + \\ + 0.5\sin(2\pi 0.5\text{time})). \quad (9)$$

Sensor capacitance is equal $C_t = \varepsilon_0 \cdot A/dt$ [F]. This creates the possibility of using adaptive algorithms to change the capacitance of the sensor itself. The control of $G(t)$ and distance d_t using such an adaptive algorithm may depend on (i) environmental E_c conditions $G(t) = f(E_c)$, (ii) the nature of the external S_e stimulus $G(t) = f(S_e)$, for which the algorithm should be implemented.

Touch simulation

The unique experiment conducted by the authors concerns the simulation of the nature of touch. You can simulate a touch that changes the effective area of the capacitor plates, given: ε_0=8.854e-12 [F/m], plate distance d=1e-3 [m], minimum plate area A_{min}=1e-5 [m²] and maximum area A_{max}=1e-4 [m²]. To simulate a touch that changes the surface A, we use the following relationship

$$A_t = A_{min} + (A_{max} - A_{min})\,(0.5 + \\ + 0.5\sin(2\pi 0.8\text{time})). \quad (10)$$

Inductive sensors detect metal objects by changes in the electromagnetic field generated by the coil (MagFES). When a metal object approaches the coil, its inductance changes and thus affects the parameters of the system, such as the oscillation frequency in the *LC* oscillator. In a dedicated mathematical model of such a sensor, its dynamic inductance

$$L(t) = L_0 - \Delta L \cdot e^{-\alpha d(t)} \quad (11)$$

where: L_0 is base inductance [H], ΔL change of inductance depending on the object, α is damping coefficient (depending on the material) and $d(t)$ distance of the object from the sensor [m].

The oscillator frequency

$$f_{OSC} = \frac{1}{2\pi\sqrt{L(t)C}}, \quad (12)$$

where: $L(t)$ is dynamic sensor inductance and C is constant capacitance in the system.

The following parameters were adopted to simulate the model of such a sensor: V_0 = 5V, base inductance L_0=10e-3[H], maximum inductance change ΔL = 5e-3 [H], damping coefficient α=10 [1/m] and capacitance C = 1e-6 [F]. The distance of the object from the sensor was experimentally determined as

$$d(t) = 0.02 + 0.01 \cdot \sin(2\pi \cdot 1 \cdot \text{time}) \text{ [m]}. \quad (13)$$

The voltage oscillates as a function of time at a frequency of f_{OSC}.

Sensor uncertainty

The authors proved that simulation of an inductive sensor model using interval calculations makes it possible to take into account uncertainties in parameters such as inductance, object distance or resistive losses. The mathematical model takes into account dynamic inductance with intervals: $L(t) \in [L_{min}, L_{max}]$, L_{min} and L_{max} are lower and upper limits of inductance uncertainty. Oscillator frequency with intervals is equal

$$f_{osc} \in \left[\frac{1}{2\pi\sqrt{L_{max}(t)C}}, \frac{1}{2\pi\sqrt{L_{min}(t)C}}\right] \quad (14)$$

The current in the sensor coil with intervals $I(t) \in V(t)/Z_{COIL}$, $Z_{COIL} = R_s + j\omega_L - j(\omega C)^{-1}$. The inductance changes sinusoidally in the $[L_{min}, L_{max}]$ range simulating dynamic conditions. The lower and upper limits of the coil impedance were calculated depending on L_{min} and L_{max}.

ICM sensor

In this sensor (inductive-capacitive model), the authors show the possibilities of using it for millisecond interactions. This study demonstrates model analysis using state variable method. Algorithm of the method is presented in Table 8 and shows the influence of the $V(t)$ source on the EcFES and MagFES elements. Analysis of the common sensor system (inductive-capacitive) over time determines the initial zero conditions and the courses of the main parameters $\mathbf{x}_1(t)$ and $\mathbf{x}_2(t)$ [34].

Let us determine the form of the state vector in operator form [35-37]. The MagFES current $i_1(t) = x_1(t)$ and the voltage on the EcFES capacitive sensor $u_c(t) = x_2(t)$ were assumed as state variables. The initial conditions were assumed for the calculations were $u_c(0\text{-}) = 0$ and $i_L(0\text{-}) = 0$. So for $t > 0$ the MagFES branch

Table 8. Algorithm for ICM

EFI³S algorithm
input: $\boldsymbol{V}(t) = V_0 \sin(2\pi f t)$ initial conditions: $\mathbf{u}_C(0-) = \mathbf{u}_C(t = t_0)$, $\mathbf{i}_L(0-) = \mathbf{i}_L(t = t_0)$, for each number IN list_of_t_numbers DO if $t < t_0$ then $\mathbf{x}_1(t) = \mathbf{i}_1(t) = \mathbf{0}(t)$ and $\mathbf{x}_2(t) = \mathbf{u}_C(t) = \mathbf{0}(t)$, if $t \geq t_0$ then $\mathbf{x}_1(t) = \mathbf{i}_1(t) = [\frac{\lvert V_m\rvert}{\lvert Z_1\rvert}\sin(\omega t + \Psi - \varphi_1) - \frac{\lvert V_m\rvert}{\lvert Z_1\rvert}\sin(\Psi - \varphi_1)e^{-\frac{R_1}{L}t}]\mathbf{1}(t)$ and $\mathbf{x}_2(t) = \mathbf{u}_C(t) = \frac{\lvert V_m\rvert}{\lvert Z_2\rvert\omega C}[\sin(\omega t + \Psi + \varphi_2 - 90^0) - \sin(\Psi + \varphi_2 - 90^0)e^{-\frac{1}{CR_2}t}]\mathbf{1}(t)$ end

$$V = R_1 i_1 + L\frac{di_1}{dt}, \tag{15}$$

and for the EcFES branch

$$V = R_2 i_2 + u_c = R_2 C\frac{du_C}{dt} + u_c. \tag{16}$$

Further transformations lead to the equation of state

$$\dot{\boldsymbol{x}}(t) = \mathbf{A}\mathbf{x}(t) + \mathbf{B}\mathbf{u}(t), \tag{17}$$

in the form

$$\begin{bmatrix} \frac{di_1}{dt} \\ \frac{du_c}{dt} \end{bmatrix} = \begin{bmatrix} -\frac{R_1}{L} & 0 \\ 0 & -\frac{1}{R_2 C} \end{bmatrix} \begin{bmatrix} i_1 \\ u_c \end{bmatrix} + \begin{bmatrix} \frac{1}{L} \\ \frac{1}{R_2 C} \end{bmatrix} [\boldsymbol{V}]. \tag{18}$$

The Laplace transform method will be used to determine the state vector.

$$\mathbf{X}(s) = [s\mathbf{1} - \mathbf{A}]^{-1}[\mathbf{B}\mathbf{V}(s) + \mathbf{X}(0)]. \tag{19}$$

In the case under consideration

$$\mathbf{X}(0) = \begin{bmatrix} i_1(0_-) \\ u_C(0_-) \end{bmatrix} = \begin{bmatrix} 0 \\ 0 \end{bmatrix}. \tag{20}$$

and determinant

$$\det[s\mathbf{1} - \mathbf{A}] = det\left\{\begin{bmatrix} s + \frac{R_1}{L} & 0 \\ 0 & s + \frac{1}{R_2 C} \end{bmatrix}\right\} = \left(s + \frac{R_1}{L}\right)\left(s + \frac{1}{R_2 C}\right), \tag{21}$$

$$[s\mathbf{1} - \mathbf{A}]^{-1} = \frac{\begin{bmatrix} s+\frac{1}{R_2 C} & 0 \\ 0 & s+\frac{R_1}{L} \end{bmatrix}}{(s+\frac{R_1}{L})(s+\frac{1}{R_2 C})} = \begin{bmatrix} \frac{1}{s+\frac{R_1}{L}} & 0 \\ 0 & \frac{1}{s+\frac{1}{R_2 C}} \end{bmatrix}. \tag{22}$$

Therefore, the operator form is as follows (for $\mathbf{v} = |V_m|\sin(\omega t + \Psi)$), and

$$\mathbf{V}(s) = \left[V_m \frac{1}{s - j\omega}\right], \tag{23}$$

$$\boldsymbol{X}(s) = \begin{bmatrix} \frac{1}{s+\frac{R_1}{L}} & 0 \\ 0 & \frac{1}{s+\frac{1}{R_2 C}} \end{bmatrix} \begin{bmatrix} V_m \frac{1}{(s-j\omega)L} \\ V_m \frac{1}{(s-j\omega)CR_2} \end{bmatrix} = \begin{bmatrix} V_m \frac{1}{(s-j\omega)(s+\frac{R_1}{L})L} \\ V_m \frac{1}{(s-j\omega)(s+\frac{1}{R_2 C})CR_2} \end{bmatrix}, \tag{24}$$

and

$$\boldsymbol{x}(t) = \left\{\mathcal{L}^{-1}\left(\begin{bmatrix} V_m \frac{1}{(s-j\omega)(s+\frac{R_1}{L})L} \\ V_m \frac{1}{(s-j\omega)(s+\frac{1}{R_2 C})CR_2} \end{bmatrix}\right)\right\}. \tag{25}$$

After calculations and transformations we have the system's response in the form

$$X_1(t) = i_1(t) = [\frac{|V_m|}{|Z_1|}\sin(\omega t + \Psi - \varphi_1) - \frac{|V_m|}{|Z_1|}\sin(\Psi - \varphi_1)e^{-\frac{R_1}{L}t}]\mathbf{1}(t), \tag{26}$$

$$X_2(t) = u_C(t) = \frac{|V_m|}{|Z_2|\omega C}[\sin(\omega t + \Psi + \varphi_2 - 90^0) - \sin(\Psi + \varphi_2 - 90^0)e^{-\frac{1}{CR_2}t}]\mathbf{1}(t), \tag{27}$$

where the internal impedance for MagFES is equal

$$|Z_1| = \sqrt{R_1{}^2 + (\omega L)^2} \text{ and } \varphi_1 = arctg(\frac{\omega L}{R_1}), \tag{28}$$

where R_1 is the sensor resistance and the internal impedance for EcFES is equal

$$|Z_2| = \sqrt{R_2{}^2 + (\frac{1}{\omega C})^2} \text{ and } \varphi_2 = arctg(\frac{1}{\omega C R_2}), \tag{29}$$

where R_2 is the sensor resistance. Model simulations are shown in the results.

RESULTS

EFHI³S

In the Figure 4a showed simulations of energy flow in a magnetic sensor inside MagFES. Additionally, they implemented energy balance there, in an interval approach. Minimum energy level (E_{min}) shows the lower limit of energy in the magnetic field with the smallest possible parameters. Maximum energy (E_{max}) shows the upper limit of energy in the magnetic field, considering the maximum possible parameters. The energy in the coil decreases due to resistive losses, which is consistent with the physics of the system. The graph shows the assumptions that the energy decreases over time, mainly due to resistive losses. The parameters (inductance, resistance) have uncertainties described by ranges. The green area shows the possible energy range over time, showing the uncertainties resulting from the parameters. Energy stored in the coil decreases over time according to the equation

$$\frac{dE(t)}{dt} = -I^2(t)Z_L \tag{30}$$

where: $I^2(t)Z_L$ these are the power losses in the coil impedance Z_L.

The energy value at subsequent moments of time is calculated as:

$$E(t+\Delta t) = E(t) + \Delta t \frac{dE(t)}{dt} \tag{31}$$

The initial energy (E_0) is stored in the magnetic field when the current in the coil is maximum and $0.5L_0I_0^2$. Both the energy output from the sensor and the sensor capacitance or inductance should be considered as an interval set.

Taking into account the uncertainties of the sensor parameters, a simulation of a capacitive sensor with intervals (Fig. 4b), located inside EcFES (on the Fig. 2). The sensor generates a signal in the form of a variable capacitance. To convert it into a current signal, electronic circuits are used that interpret the changes in capacitance and convert them to a current proportional to the measured value. Both the variable energy of the magnetic sensor and the variable capacitance of the capacitive sensor enable simultaneous hybrid use and generation of a signal response to the realized touch.

Sensor peaks

Simulation of signal processing from a capacitive sensor is shown in Figure 5a. The capacitance (C_t) changes dynamically over time, simulating the sensor's operation. Capacitance changes are a sinusoidal simulation. Frequency/voltage (V_t) corresponds to capacitance changes and is linearly scaled. A certain specific capacitance value corresponds to the maximum voltage, which indicates the maximum output current from the V/I converter. This current signal is further converted in the CU module into a decision directed to the IoT [38-40]. The current peaks correspond to minimum sensor capacitance levels and maximum voltage levels.

A certain specific capacitance value corresponds to the maximum voltage, which indicates the maximum output current from the V/I converter. Current signal optimization involves improving its quality, precision, and usability to minimize information loss and maximize data utilization. For the graph on Figure 5b a shaded area

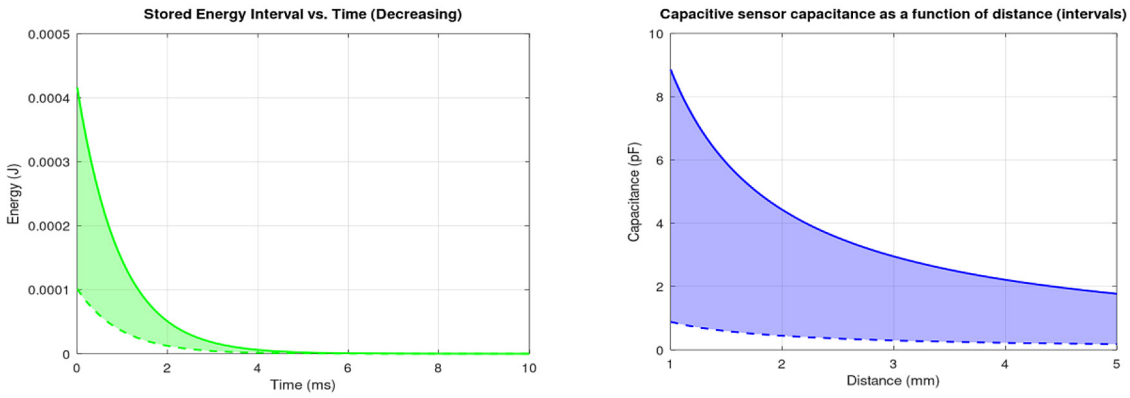

(a) (b)

Figure 4. Energy flow simulating graph in the magnetic sensor with intervals (a), and the capacitive sensor simulation with intervals (b)

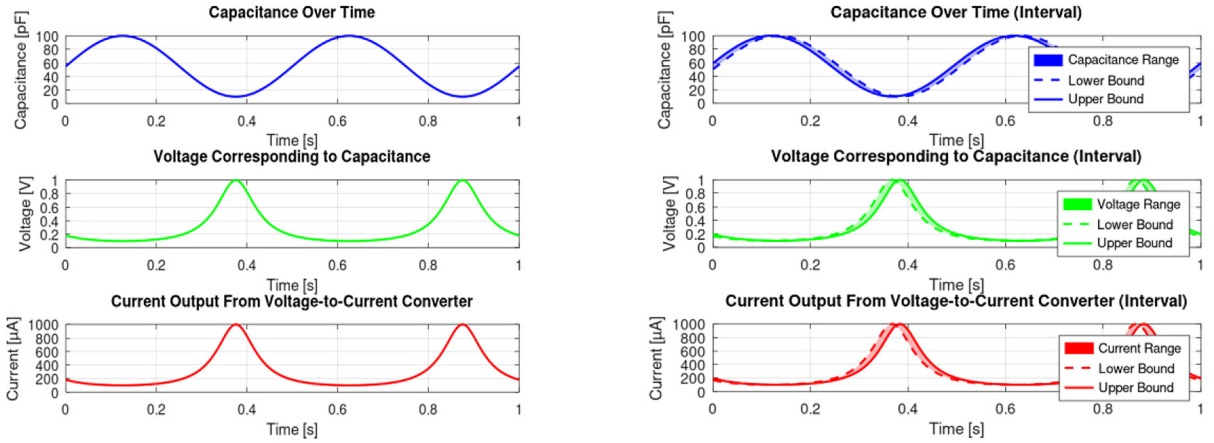

(a) basic line (b) for intervals

Figure 5. Simulation for converting a capacitive sensor signal to a current signal

representing the interval range of capacitance with dashed and solid lines for lower and upper bounds. The graph shows the voltage range corresponding to capacitance, with bounds clearly marked. Shaded interval range for current show how capacitance variability propagates through the system for flexibility in response.

Harmonic sensor capacitance

As you can see on the Figure 6, the capacitance changes over time, which affects the current characteristics – the current amplitude increases over time, above the level of 100 nA (green colour). The current changes dynamically depending on the voltage and capacity, reflecting the actual operating conditions of the sensor.

Conversely, the dynamic reduction of the sensor capacitance, represented by a nonlinear process (red curve), leads to a reduction of the sensor current to at least the level of 100 nA (green colour). Therefore, the dynamic change of the sensor property leads to its curvilinear current response, constituting a control signal to its IoT environment.

Distance between capacitor plates

As our experiments show, you can change the distance between the capacitor plates, which affects the capacitance (Fig. 7a). For this model and the mentioned data, the simulation shows that the sensor capacity decreases as the distance increases.

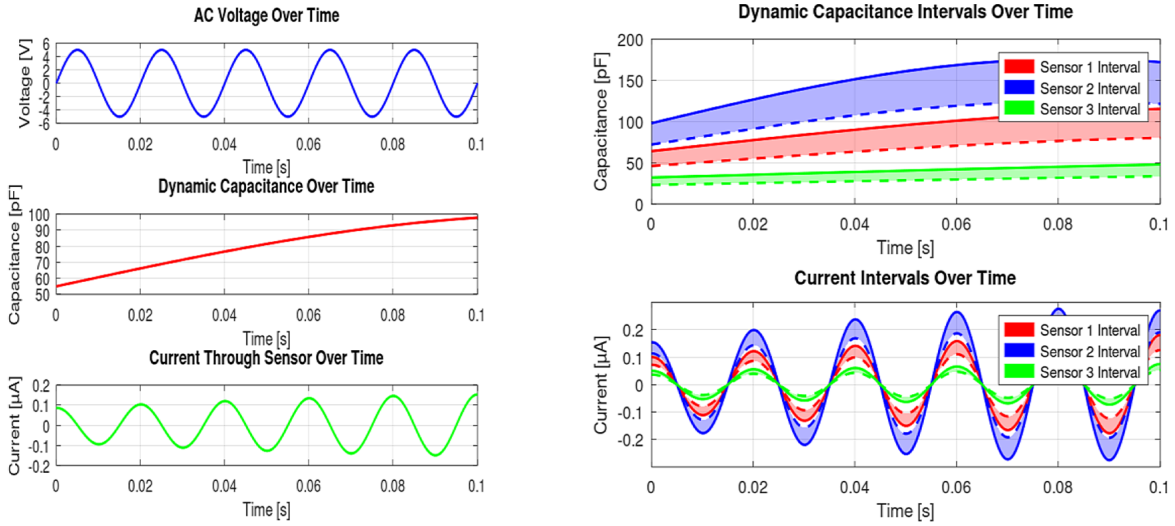

Figure 6. Dynamic response of the capacitive sensor to $V(t)$ input

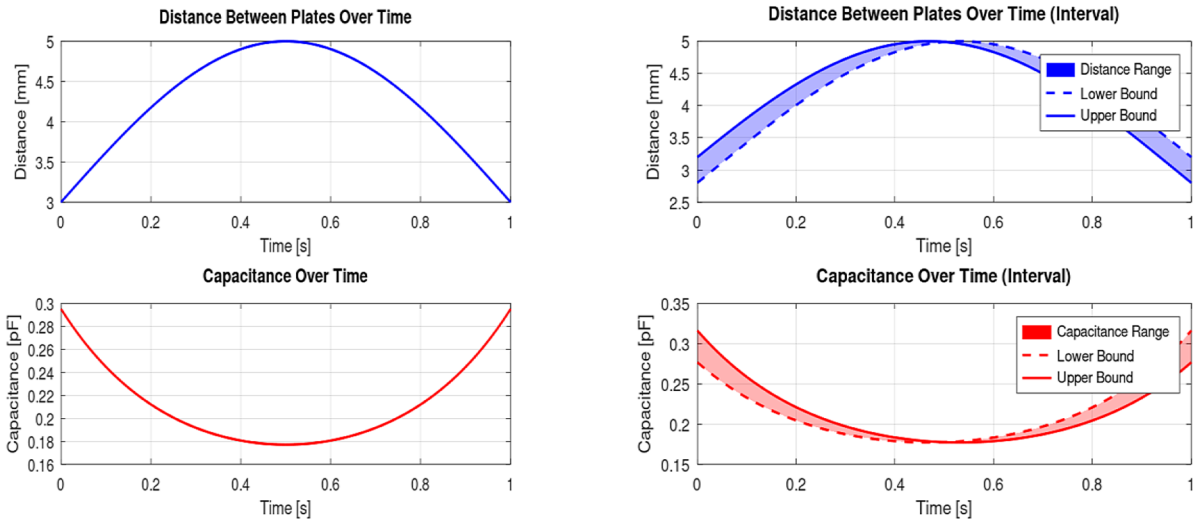

(a) basic graph (b) interval option

Figure 7. The dynamic effect of changing the distance between the capacitor plates on the sensor capacity

As we can see, this change and this impact are not directly proportional. The authors' key insights are that the interval approach (Fig. 7b) provides a realistic representation of the system's behavior, accounting for possible deviations in the distance between the plates. An increase of the distance by 1 mm from 3 to 4 mm causes a non-linear decrease of the sensor capacitance from 0.295 pF to 0.21 pF. In turn, a reduction of the distance from 5 mm to 4 mm leads to an increase of the sensor capacitance from about 0.18 pF to about 0.22 pF.

Touch simulation and sensor uncertainty

Touch can be simulated, which changes the effective area of the capacitor plates (Fig. 8). The gradual change of plate area over time and alternating leads to alternating changes of capacitance over time. The dynamics of changes is as follows: changing the effective plate area from 0.6 to 0.8 cm^2 causes the capacitance to change from 0.5 pF to over 0.5 pF. The dynamics of the changes are as follows: changing the effective plate area from 0.6 to 0.8 cm^2 causes a change in capacitance from 0.5 to over 0.7 pF. Therefore, a larger surface imprint on the sensor corresponds to a relatively higher sensor capacitance, which translates into a current signal to the IoT environment. Now the question arises, what will happen when the touch has too large a surface. In such a case, it would be necessary to provide an adaptive algorithm to reduce the sensor response signal to the IoT environment, depending on its nature.

The dynamic inductance and oscillator frequency are visualized in Figure 9. The object distance $d(t)$ varies sinusoidally, simulating the object's movement relative to the sensor. The dynamic inductance $L(t)$ decreases exponentially with decreasing object distance. The oscillator frequency f_{osc} increases with decreasing inductance. The voltage oscillations reflect the changes in the LC circuit. As a result of the presented modeling, the sinusoidal change in distance simulates the dynamic movement of the object. The inductance decreases exponentially as the object approaches. The voltage oscillations change their frequency proportionally to the dynamic changes in inductance.

The authors further demonstrated the influence of Gaussian noise on the energy effect of a single sensor. The effect of noise on energy was negligible. In Figure 8 effective plate area compares the ideal area (solid line) with the noisy area (dashed green line). Capacitance shows how Gaussian noise affects the property, with a solid red line for the ideal values and a dashed black line for the noisey values. The lower graph illustrates the energy stored in the capacitor, comparing the ideal energy (solid magenta line) with the noisy energy (dashed cyan line).

The model shows how changes in the distance of a metal object affect the inductance and voltage oscillations in an LC circuit (sensors used without contact). The first graph in blue shows the slow nonlinear increase of distance of metal object over time. The corresponding nonlinear increase of inductance over time is shown in black.

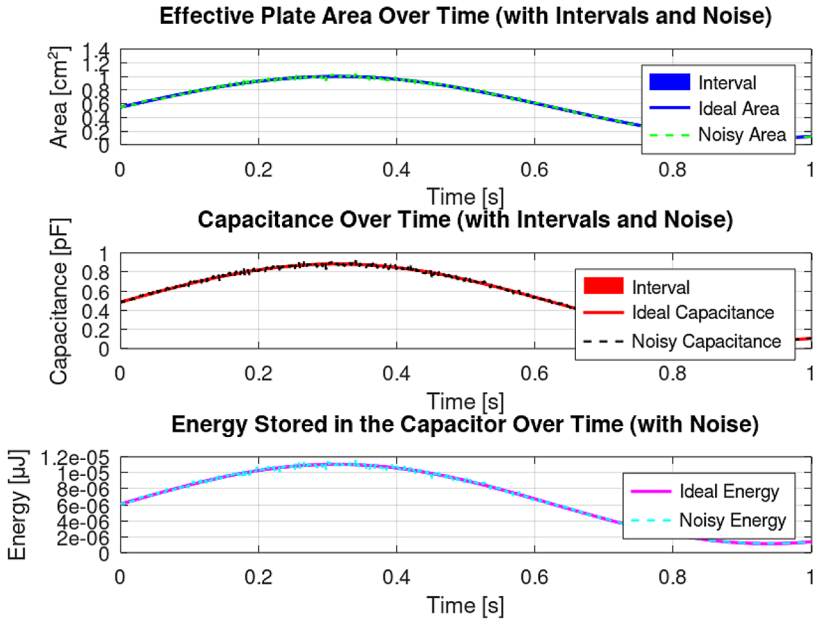

Figure 8. Simulating touch changing the surface and capacitance of the sensor

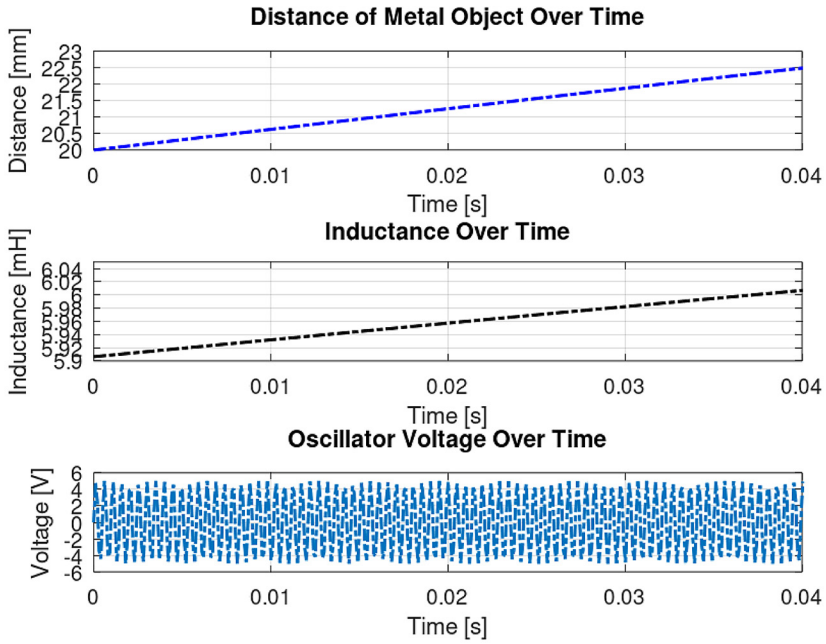

Figure 9. Inductive sensor simulation

It corresponds to the non-linear slow increase of inductance over time.

ICM model

The results of the hybrid sensor is shown in Figure 10. The modeling assumed: V_m=5[V], f=50[Hz], C=1e-6[F], L=1e-3[H]. As we can see, the current of the MagFES sensor follows the increase of the input voltage V(t).

The scale on the time axis indicates that we are moving in millisecond ranges. Therefore, such hybrids can be used at higher frequencies, because they will react to the quickly changing environment.

The presented figure shows that the sensor current is small, on the order of a fraction of mA, so it can be successfully used in such systems. Its value increases in response to the decreasing wave of the input signal to a certain extent and

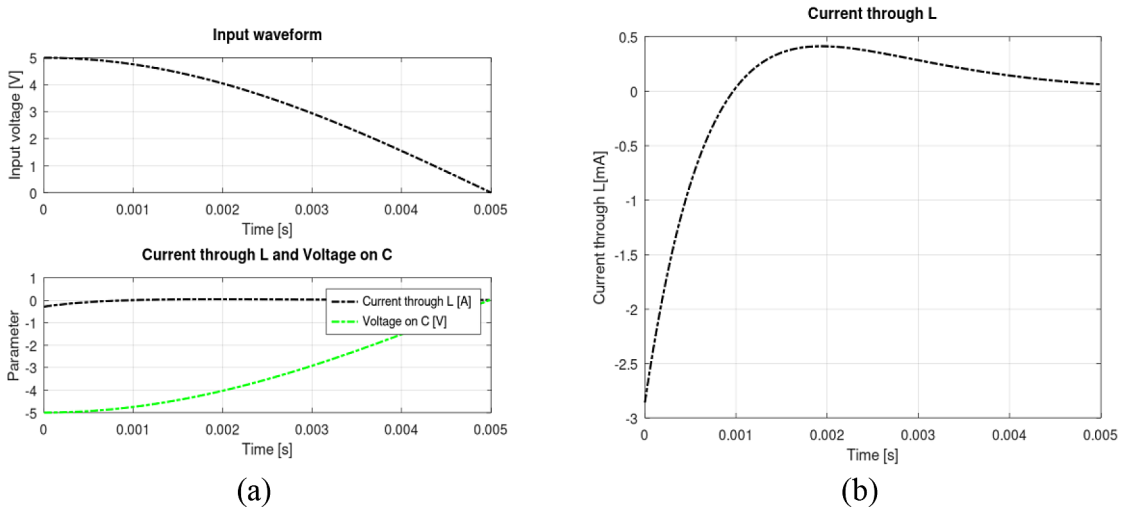

Figure 10. Hybrid sensor parameters: (a) the voltage for EcFES and (b) the current for MagFES

stabilizes. The corresponding capacitance sensor signal does not stabilize and shows negative dynamics of about -1.0V/1ms.

DISCUSSION

EFHI³S model

First, our results indicate that it is possible to control the sensor energy flow (Equation 30) over time in a dissimilar sensor array. This flow can be adjusted by changing the signal frequency or by interval control of the MagFES parameters. This process is important because it involves techniques to minimize and control energy consumption, increase efficiency, and optimize power and energy storage methods [41, 42].

Second, we propose that it is possible to generate an interval signal by a sensor array, meaning that the variable energy of the magnetic sensor and the variable capacitance of the capacitive sensor enable simultaneous hybrid use at the same time instant and generation of a signal response as realized touch.

Sensor peaks

We managed to show that it is possible to obtain capacitive sensor parameters whose peak values correspond to the minimum capacitance levels of the sensor and the maximum voltage levels. In this way, we know a priori the current peaks at the microampere level and we can predict them in order to select the level of adaptation of the sensors on the matrix. Peak detection is an approach that reduces energy costs. A similar sentence was shown in [43, 44]. We were able to demonstrate that it is possible to select more optimal parameters of the sensors on the matrix [45, 46] as also suggested in the work [47].

A potential threat from the environment here is interference with the sensor. The challenge is to ensure the safety and the most undisturbed operation of the sensor array. Therefore, it requires ensuring the security of the entire system. The authors additionally suggested the concept of response flexibility for the sensor (Fig. 5b). This flexibility is provided by the interval approach, when sensor 1 changes the parameters C_{min} = 10 pF to C_{max} = 100 pF, sensor 2 – C_{min} = 20 pF to C_{max} = 150 pF and sensor 3 – C_{min} = 5pF to C_{max} = 50 pF. This interval approach to designing smart sensors: increases the reliability and flexibility of sensors, takes into account the uncertainty of parameters and conditions, enables better design optimization, promotes integration with IoT and AI systems, reduces the risk of failures and improves the validation process. This approach opens new possibilities for smart measurement systems, increasing their adaptability and precision in dynamic environments.

Harmonic sensor capacitance

It is possible to indicate the ranges of dynamic capacitance over time for which the generated sensor signal will have, based on the harmonic source, a tendency of increasing current response amplitude at the level of nanoamps and tens of picofarads (Fig. 7a). This study showed that the

transition from the green sensor to the red and then to the blue one (Fig. 7b) is characterized by increasing capacitance, which corresponds to a higher amplitude of the signal response. Therefore, by algorithmically controlling, for example, capacitive trimmers, one can induce differences in the control signals coming from the sensors. There is an inflection point for the interval representation to which the distance between plates can be reduced.

Distance between capacitor plates

Key insights are that the interval approach provides a realistic representation of the system's behavior, accounting for possible deviations in the distance between the plates. Dynamic behavior and variations in capacitance over time due to distance changes are explicitly shown, which is crucial for designing robust sensors with practical applications. This study showed that there is an inflection point for the interval representation to which the distance between plates can be reduced.

Touch simulation and sensor uncertainty

A study shows the impact of Gaussian noise on the touch of the sensor (Fig. 8). This is an important issue in many cases when the sensor may become dirty. Gaussian noise in the context of a touch sensor represents random fluctuations or variations in the sensor's signal due to environmental, material, or electronic noise sources. It typically follows a normal distribution (bell-shaped curve) and affects the reliability and accuracy of the sensor's output. In our simulation, noise introduces small, unpredictable variations in measurements, such as changes in the effective plate area, capacitance, or energy stored in the system. This can make it difficult to distinguish between intentional touch inputs and noise-induced variations. Reduced Sensitivity results from the fact that noise can mask subtle changes caused by a light touch, leading to reduced sensitivity.

The chart shows that small signal variations might be perceived as part of the noise floor, making weak interactions harder to detect. Additionally, the authors noted that false positives occur when the noise mimics a legitimate touch signal. False negatives occur when a valid touch signal is obscured by noise, leading to missed detection.

Gaussian noise reduces the accuracy of the sensor's measurements. For instance effective plate area variations might incorrectly suggest different pressure or touch intensity. Capacitance noise may lead to incorrect position or contact force estimation to sensor area. Especially with very small sensor contact surfaces or delicate stimuli.

The work [48] presents the concept of developing energy generation from the e-Skin hand area alone, over 100W, with a body area of approximately 1.5 m^2. With this assumption, if the hand surface of 8400 mm^2 was covered with e-skin and if each sensor (C = 1 μF) consumes E_c= 0.5·1e-6·0.5·0.5 = 0.125 μW of power over 1s time. If the hand surface of 8400 mm^2 was covered with e-skin and if each sensor consumes 0.125 μW of power, the sensor hand would consume 8400×0.125 = 1050 μW so about 1 mW. This seems to be sufficient, assuming also the use of multisensors at the nodal points of the mesh covering the artificial hand.

Distance 0.75mm corresponds to an increase of inductance of 20 μH changing the voltage f_{osc}. Such a sensor built into the skin allows for non-contact detection of the metal surface with high sensitivity. Based on the change in frequency, the sensor recognizes that a metal object has entered its range. The simulations we performed show that the maximum current and minimum current should be predicted for each sensor of the matrix separately.

ICM model

The voltage on the EcFES sensor drops the more the input voltage increases, which is mainly caused by the exponential factor (Fig. 10). This proves that capacitive sensors are versatile and increasingly applied in advanced and emerging fields due to their high sensitivity, low power consumption, and ability to detect various physical and chemical properties in a short time (here we have milliseconds). Such models can be transferred to the scale of nanogenerators and used to work with them. We modelled this sensor as a hybrid structure.

The proposed technique in [49-51] uses both the inductance and stray capacitance of the planar coil, but works in a different structure and scheme. In our study we have two two-sensor circuits partially connected to each other as shown by Equations (26) and (27). Therefore, the expectations for such a hybrid are different. It was noted that for the presented graphs the current of the MagFES sensor follows the input voltage. For

the presented graphs the current of the MagFES sensor goes the opposite way to the input voltage and with different tracking dynamics. Such a multifunctional sensor allows for simultaneous point application to the local area, generating two signals simultaneously, detecting the human body and a metal surface.

Moreover, an interesting property has been shown, looking at Figure 10b, that the sensor current for $t = 1$ ms changes direction to the right or left, while the input signal is dynamically decreasing what is an interesting property of a multisensor. The tendency of object recognition requires the adaptation of capacitance and inductance, therefore, further research on adaptive control algorithms in such hybrid systems with adapted sensitivity detection is important.

The works [52, 53] confirm the importance of such integrated systems and can be used for physical human-robot interaction or for the detection of metal-lubricant materials. The fine detection of oil abrasive particles in mechanical equipment is crucial to the fault determination of the equipment, especially when particles of two different materials are mixed through the sensor.

CONCLUSIONS

The presented research highlights the significant potential of intelligent skin sensors in enhancing the functionality and safety of autonomous systems integrated with IoT. Using a hybrid approach involving capacitive-inductive integrated sensors, the proposed modeling techniques demonstrate both energy dynamics and signal processing issues. The interval-based representation of sensor parameters enables a more robust and flexible design that accounts for environmental uncertainties and changes.

Simulations demonstrated the dynamic interaction of energy flow in the magnetic sensor and capacitance changes in the capacitive sensor, revealing key insights into their individual and hybrid behaviours. Key findings include that the magnetic sensor exhibits predictable energy dissipation. The capacitive sensor dynamically responds to capacitance changes induced by external factors such as plate distance and touch simulation, enabling precise signal generation and current optimization.

The interval modeling approach enhances the reliability and adaptability of the sensors, ensuring consistent performance under different conditions. Notably, the introduction of Gaussian noise simulation provides a realistic understanding of the sensor behavior in practical operational scenarios such as environmental pollution or signal interference.

The hybrid nature of the proposed smart sensors enables simultaneous detection of multiple parameters such as human touch and presence of metallic objects, making them suitable for applications in advanced robotics, human-machine interfaces, and environmental monitoring. Furthermore, the findings highlight the importance of adaptive control algorithms to optimize sensor response, especially in dynamic and uncertain environments.

This work provides a foundation for further exploration of integrated intelligent sensor systems, promoting their use in IoT-enabled applications requiring very high sensitivity, precision, and energy efficiency and in the THz frequency band. Further research will focus on improving the adaptive algorithms and extending the capabilities of such multi-sensors to nano-scale applications.

REFERENCES

1. Chen J., Zhu Y., Chang X., Pan D. et al. Recent progress in essential functions of soft electronic skin, Advanced Functional Materials 2021, 31(42), 2104686. https://doi.org/10.1002/adfm.202104686
2. Li W., Ke K., Jia J. et al. Recent advances in multiresponsive flexible sensors towards e-skin: a delicate design for versatile sensing, Small 2021, 18(7), 2103734. https://doi.org/10.1002/smll.202103734
3. Wang X., Dong L., Zhang H. et al. Recent progress in electronic skin, Advanced Science 2015, 2(10), 1500169. https://doi.org/10.1002/advs.201500169
4. Liu Y., Wang L., Zhao L. et al. Recent progress on flexible nanogenerators toward self-powered systems, light advanced manufacturing 2020, 2, 318-340. https://doi.org/10.1002/inf2.12079
5. Shih B., Shah D., Li J. et al. Electronic skins and machine learning for intelligent soft robots, Science Robotics 2020, 5(41). https://doi.org/10.1126/scirobotics.aaz9239
6. Lu N., Kim D., Flexible and stretchable electronics paving the way for soft robotics, soft robotics 2013, 1(1). https://doi.org/10.1089/soro.2013.0005
7. Shu S., Wang Z., Chen P. et al. Machine-learning assisted electronic skins capable of proprioception and exteroception in soft robotics, Advanced

Materials 2023, 35(18). https://doi.org/10.1002/adma.202211385

8. Hedge Ch., Su J., Tan J. Sensing in soft robotics, ACS Nano 2023, 17(16). https://pubs.acs.org/doi/full/10.1021/acsnano.3c04089
9. Ma Y., Li H., Chen S. et al. Skin-like electronics for perception and interaction: materials, structural designs, and applications, Advanced Intelligent Systems 2020, 3(4). https://doi.org/10.1002/aisy.202000108
10. Yang J., Mun J., Kwon S. et al. Electronic skin: recent progress and future prospects for skin-attachable devices for health monitoring, robotics, and prosthetics, Advanced Materials 2019, 31(48), 1904765. https://doi.org/10.1002/adma.201904765
11. Liu X., Wei Y., Qiu Y. et al. Advanced flexible skin-like pressure and strain sensors for human health monitoring, Micromachines 2021, 12(6), 695. https://doi.org/10.3390/mi12060695
12. Shimadera S., Kitagawa K., Sagehashi K. Optical skin: sensor-integration-free multimodal flexible sensing, Computer Vision and Pattern Recognition 2022, 12, 13096. https://doi.org/10.48550/arXiv.2202.03189
13. Liu Z., Cai M., Hong S. et al. Inverse design of artificial skins, Soft Matter 2023. https://doi.org/10.48550/arXiv.2304.04609
14. Zhang L., Pan J. Zhang Z. et al. Ultrasensitive hybrid optical skin, Applied Physics 2018. https://doi.org/10.48550/arXiv.1812.03808
15. Zhang L., Pan J. Zhang Z. et al. Ultrasensitive skin-like wearable optical sensors based on glass micro/nanofibers, Opto-Electronic Advances 2020, 3(190022). DOI: 10.29026/oea.2020.190022
16. Liu Y., Pharr M., Salvatore G. et al. Lab-on-skin: a review of flexible and stretchable electronics for wearable health monitoring, ACS Nano 2017, 11(10) 9567-9569. https://doi.org/10.1021/acsnano.7b07214
17. Liu S., Guo W., Chen H. et al. Recent progress on flexible self-powered tactile sensing platforms for health monitoring and robotics, Small 2024. https://doi.org/10.1002/smll.202405520
18. Yuan Z., Han S., Gao W. et al. Flexible and stretchable strategies for electronic skins: materials structure and integration, ACS Appl. Electron. Mater. 2022, 4(1),1-26. https://doi.org/10.1021/acsaelm.1c00025
19. Ma Y., Li H., Chen S. et al. Skin-like electronics for perception and interaction: materials, structural designs, and applications, Advanced Intelligent Systems 2020, 3(4). https://doi.org/10.1002/aisy.202000108
20. Nie B., Liu S., Qu Q. et al. Bio-inspired flexible electronics for smart e-skin, Acta Biomaterialia 2022, 139, 280-295. https://doi.org/10.1016/j.actbio.2021.06.018
21. Someya T., Yokota T., Lee S. Electronic skins for robotics and wearables, IEEE 33rd International Conference on Micro Electro Mechanical Systems (MEMS), Vancouver, Canada, January 2020. https://doi.org/10.1109/MEMS46641.2020.9056304
22. Liu H., Wu Ch., Lin S. From skin movement to wearable robotics: the case of robotic gloves, Soft Robotics 2024, 11(5). https://doi.org/10.1089/soro.2023.011
23. Zhong Ch., Zhao S., Liu Y. et al. A flexible wearable e-skin sensing system for robotic teleoperation, Robotica 2023, 41(3), 1025-1038. https://doi.org/10.1017/S026357472200131X
24. Liu X., Li H., Tao M. et al. Organic flexible electronics for innovative applications in electronic skin, Advanced Materials Technologies 2024, 1-26. https://doi.org/10.1002/admt.202400661
25. Zhu P., Li Z., Pang J. et al. Latest developments and trends in electronic skin devices, Soft Sci. 2024, 4(17). http://dx.doi.org/10.20517/ss.2024.05
26. Zhou Z., Xu Z., Cao L. et al. Triboelectricity based self-powered digital displacement sensor for aircraft flight actuation, Advanced Functional Materials, 2023, https://doi.org/10.1002/adfm.202311839
27. Zhang Y., Chen Q., Zhang F. Electrochemical triboelectricity: A comprehensive survey of current research and future prospects, Nano Energy 2024, 130, 110180. https://doi.org/10.1016/j.nanoen.2024.110180
28. Jiang Q., Antwi-Afari M., Fadaie S. Self-powered wearable internet of things sensors for human-machine interfaces: a systematic literature review and science mapping analysis, Nano Energy 2024, 131 (A), 110252. https://doi.org/10.1016/j.nanoen.2024.110252
29. Juyal S., Sharma S., Shukla A. Smart skin health monitoring using AI-enabled cloud-based IoT, Materials Today 2021, 46(20), 10539-10545. https://doi.org/10.1016/j.matpr.2021.01.074
30. El Fray I., Wiliński A. Modifications of the formal risk analysis and assessment for the information system security, Advances in Science and Technology Research Journal 2024, 18(2), 317-332. DOI:10.12913/22998624/185162
31. Bartłomiejczyk M., El Frey I., Kurkowski M. et al. User authentication protocol based on the location factor for a mobile environment, IEEE Access 2022, 10, 16439-16455. https://doi.10.1109/ACCESS.2022.3148537
32. Pasko M. Przyklady i zadania z dynamiki elektrycznych obwodow liniowych. Wydawnictwo Politechniki Slaskiej, 2003. ISBN: 83-7335-079-9
33. Houpis C.H., Sheldon S.N. Linear control system analysis and design with matlab, CRC Press, 2013. https://doi.org/10.1201/b16032

34. Wegrzyn S. Rachunek operatorowy, PWN, 1960
35. Wagner K. Rachunek operatorowy i przekształcenie Laplacea, PWN, 1960
36. Hillar G. MQTT essentials - a lightweight IoT protocol, Packt Publishing Ltd., Birmingham, 2017.
37. Zhao J., Sun L., Fan H. et al. MQTT-based internet of things smart home linkage control system, 2024 3rd International Conference on Electronics and Information Technology (EIT), Chengdu, China, 2024, 521-525. https://doi.org/10.1109/EIT63098.2024.10762564.
38. Yassein M., Shatnawi M., Aljwarneh S et al. Internet of things: survey and open issues of MQTT protocol, 2017 International Conference on Engineering & MIS (ICEMIS), Monastir, Tunisia, 2017, 1-6. DOI: 10.1109/ICEMIS.2017.8273112.
39. Singh M., Rajan M., Shivraj V. et al. Secure MQTT for internet of things (IoT), 2015 Fifth International Conference on Communication Systems and Network Technologies, Gwalior, India, 2015, 746-751. https://doi.org/10.1109/CSNT.2015.16.
40. Smart G. Practical python programming for IoT, Packt Publishing Ltd., Birmingham, 2020. ISBN 978-1-83898-246-1
41. Yu J., Tang J., Wang L. et al. Dual-mode sensor for intelligent solution monitoring: Enhancing sensitivity and recognition accuracy through capacitive and triboelectric sensing, Nano Energy, 2023, 118. https://doi.org/10.1016/j.nanoen.2023.109009
42. Ren H., Zhang H. Control strategy based on improved fuzzy algorithm for energy control of wrist rehabilitation robot, Alexandria Engineering Journal, 2023, 77, 634-644. https://doi.org/10.1016/j.aej.2023.07.024.
43. Kumar L., Islam T., Mukhopadhyay S., Sensitivity enhancement of a PPM level capacitive moisture sensor, Electronics 2017, 6(2). https://doi.org/10.3390/electronics6020041
44. Zeng Y., Qin Y., Yang Y. et al. A Low-Cost Flexible Capacitive Pressure Sensor for Health Detection, 2022, 22(8). https://doi.org/10.1109/JSEN.2022.3158354
45. Cheng A., Wu L., Sha Z, Recent advances of capacitive sensors: materials, microstructure designs, applications, and opportunities, Advanced Materials Technologies, 2023. https://doi.org/10.1002/admt.202201959
46. Mohamed F. Hassan, Patrick K., Capacitive polymer sensors: factors influencing performance and design principles, Sensors and Actuators, 2023(393). https://doi.org/10.1016/j.snb.2023.134211
47. Litvinov A., Etrekova K., Podlepetsky et al. MOSFE-Capacitor Silicon Carbide-Based Hydrogen Gas Sensors, Sensors 2023, 23(7), 3760. https://doi.org/10.3390/s23073760
48. Escobedo P., Ntagios M., Shakthivel D. et al. Energy generating electronic skin with intrinsic tactile sensing without touch sensors, IEEE Transactions on Robotics, 2021, 37(2), 683-690. https://doi.org/10.1109/TRO.2020.3031264
49. Yin X., Zhang X., Li Y. *et al*. A combined inductive and capacitive non-destructive evaluation technique using a single spiral coil sensor, *IEEE Sensors Journal*, 2021, 21(16), 18187-18196. https://doi.org/10.1109/JSEN.2021.3084204
50. Wiliński A., Hoser P., Strzęciwilk D. et al. Modeling nonlinear response of the humanoid's sensory lobe to environmental threats, Computer Algebra Systems in Teaching and Research (CASTR), Siedlce, 2024 (XIII), 155-171. ISBN 978-83-68355-03-1
51. Wiliński A., Strzęciwilk D., Hoser P. Modeling the estimation of the impedance response of Artificial skin to sensory stimulation, Computer Algebra Systems in Teaching and Research (CASTR), Siedlce, 2024 (XIII), 172-184.
52. Yim H., Kang H., Moon S. et al. Multi-functional safety sensor coupling capacitive and inductive measurement for physical human–robot interaction, Sensors and Actuators, 2023, 354(114285). https://doi.org/10.1016/j.sna.2023.114285
53. Xie Y., Wang S., Zhang S. et al. Dual Inductive–Capacitive Detection Cell: A Promising Tool for Distinguishing Mixed Metal Particles, *IEEE Sensors Journal*, 2023, 23(18), 21163-21171. https://doi.org/10.1109/JSEN.2023.3303914